CMS Physics Analysis Summary

Contact: cms-pag-conveners-higgs@cern.ch 2012/11/14

Search for the standard model Higgs boson produced in association with W or Z bosons, and decaying to bottom quarks

The CMS Collaboration

Abstract

A search for the standard model Higgs boson (H) decaying to $b\bar{b}$ when produced in association with a weak vector boson (V) is reported for the following modes: W($\mu\nu$)H, W($e\nu$)H, Z($\mu\mu$)H, Z(ee)H and Z($\nu\nu$)H. The search is performed in data samples corresponding to integrated luminosities of 5.0 fb^{-1} at $\sqrt{s}$ =7 TeV and 12.1 fb^{-1} at $\sqrt{s}$ =8 TeV, recorded by the CMS experiment at the LHC. Upper limits, at the 95% confidence level, on the VH production cross section times the $H \to b\bar{b}$ branching ratio, with respect to the expectations for a standard model Higgs boson, are derived for a Higgs boson in the mass range 110-135 GeV. In this range, the observed upper limits vary from 1.0 to 4.2 times the standard model prediction; the corresponding expected limits vary from 0.9 to 1.9. At a Higgs boson mass of 125 GeV the observed limit is 2.5 and the expected limit is 1.2. An excess of events is observed above the expected background with a local significance of 2.2 standard deviations, which is consistent with the expectation from the production of the standard model Higgs boson.

1 Introduction

The CMS and ATLAS collaborations have recently reported the discovery of a new boson [1, 2], with a mass, m_{H}, near 125 GeV and with properties, so far, compatible with those of the standard model Higgs boson [3–8]. To this date significant signals have been observed in channels where the boson decays into $\gamma\gamma$, ZZ and WW pairs. At a mass of 125 GeV the standard model Higgs boson decays predominantly into a bottom-antibottom quark pair ($\mathrm{b\bar{b}}$). The observation and study of the $\mathrm{H} \to \mathrm{b\bar{b}}$ decay is essential in determining the nature of the newly discovered boson. The CDF and D0 collaborations have reported, also recently, evidence for an excess of events, at the 3.1 standard deviation level, in the search for the standard model Higgs boson when produced in association with a weak vector boson and decaying to $\mathrm{b\bar{b}}$ [9–11]. The excess is most significant in the 120–135 GeV mass range.

In this note a search for the standard model Higgs boson in the $\mathrm{pp} \to \mathrm{VH}$ production mode is presented, where V is either a W or a Z boson and $\mathrm{H} \to \mathrm{b\bar{b}}$. The search is performed in data samples corresponding to integrated luminosities of 5.0 fb^{-1} at $\sqrt{s} = 7$ TeV and 12.1 fb^{-1} at $\sqrt{s} = 8$ TeV, recorded by the CMS experiment at the LHC. The following final states are included in the search: $\mathrm{W}(\mu\nu)\mathrm{H}$, $\mathrm{W}(e\nu)\mathrm{H}$, $\mathrm{Z}(\mu\mu)\mathrm{H}$, $\mathrm{Z}(ee)\mathrm{H}$ and $\mathrm{Z}(\nu\nu)\mathrm{H}$, all with the Higgs boson decaying to $\mathrm{b\bar{b}}$. Backgrounds arise from production of W and Z bosons in association with jets (from all quark flavors), singly and pair-produced top quarks ($\mathrm{t\bar{t}}$), dibosons and QCD multijet processes. The analysis presented here contains more 8 TeV data and includes some modifications with respect to the previous CMS Higgs boson search in these final states [12]. The main changes are the explicit inclusion of soft-lepton information in the treatment of the measurement of the energy associated with jets originating from b quarks, and the inclusion of a new category of events from the high $p_{\mathrm{T}}(\mathrm{V})$ region in which the b-tagging requirements are looser.

Simulated samples of signal and backgrounds are used to provide guidance in the optimization of the analysis. Control regions in data are selected to adjust the event yields from simulation for the main background processes and to estimate their contribution in the signal region. Upper limits at the 95% confidence level (CL) on the $\mathrm{pp} \to \mathrm{VH}$ production cross section times the $\mathrm{H} \to \mathrm{b\bar{b}}$ branching ratio are obtained for Higgs boson masses in the 110–135 GeV range. These limits are extracted by fitting the shape of the distribution of the output discriminant of a boosted-decision-tree (BDT) algorithm [13] for the presence of a Higgs boson signal above what is expected from all background components.

2 Simulations

Simulated samples of signal and backgrounds are produced using various event generators, with the CMS detector response modeled with GEANT4 [14]. The Higgs boson signal samples are produced using the POWHEG [15] event generator interfaced with HERWIG++ [16] for parton showering and hadronization. The diboson samples are generated with PYTHIA 6.4 [17]. The MADGRAPH 5.1 [18] generator is used for the W+jets, Z+jets, and $\mathrm{t\bar{t}}$ samples. The single-top samples are produced with POWHEG and the QCD multijet samples with PYTHIA. The default set of parton distribution functions (PDF) used to produce the Next-to-Leading-Order (NLO) POWHEG samples is the NLO CTEQ6M [19] while the Leading-Order (LO) CTEQ6L1 [19] is used for the rest of the samples, which come from LO calculations. The PYTHIA parameters for the underlying event are set to the Z2 tune [20] for the 7 TeV samples and to Z2Star [20] for the 8 TeV samples.

During the 2011 data taking period the LHC instantaneous luminosity reached up to 3.5 $\times$

$10^{33}\text{cm}^{-2}\text{s}^{-1}$ and the average number of pp interactions per bunch crossing was approximately ten. During the 2012 period considered here the LHC instantaneous luminosity reached $7.5 \times 10^{33}\text{cm}^{-2}\text{s}^{-1}$ and the average number of pp interactions per bunch crossing was approximately 14. Additional pp interactions overlapping with the event of interest in the same bunch crossing, denoted as pile-up events (PU), are therefore added in the simulated samples to represent the PU distribution measured in data.

3 Triggers

Several triggers are used to collect events consistent with the signal hypothesis in all five channels. For the WH channels the trigger paths consist of several single-lepton triggers with tight lepton identification. Leptons are also required to be isolated from other tracks and calorimeter energy depositions to maintain an acceptable trigger rate. For the $\text{W}(\mu\nu)\text{H}$ channel, for the 2011 data set, the trigger thresholds for the muon transverse momentum, p_T, are in the range of 17 to 40 GeV. The higher thresholds are used for the periods of higher instantaneous luminosity. For the 2012 data set the muon p_T trigger thresholds were set at 24 GeV for the single isolated-muon trigger. A single muon trigger with a 40 GeV p_T threshold was also used, without any isolation requirements. The combined single-muon trigger efficiency is $\approx 90\%$ for signal events that pass all offline requirements that are described in Section 5. For the $\text{W}(\text{e}\nu)\text{H}$ channel, for the 2011 data set, the electron p_T threshold ranges from 17 to 30 GeV. The lower-threshold paths require two jets and a minimum requirement, in the 15–25 GeV range, on the norm of an online estimate the missing transverse energy vector, defined as the negative vector sum of the transverse momenta of all reconstructed jets identified by a particle-flow algorithm [21]. These extra requirements help to maintain acceptable trigger rates during the periods of high instantaneous luminosity. For the 2012 data set, the single isolated-electron trigger uses a 27 GeV threshold. The combined efficiency for these triggers for signal events that pass the final offline selection criteria is $>95\%$.

The $\text{Z}(\mu\mu)\text{H}$ channel uses the same single-muon triggers as the $\text{W}(\mu\nu)\text{H}$ channel. For the $\text{Z}(\text{ee})\text{H}$ channel, dielectron triggers with lower p_T thresholds (17 and 8 GeV) and tight isolation requirements are used. These triggers are $\approx 99\%$ efficient for all ZH signal events that pass the final offline selection criteria. For the $\text{Z}(\nu\nu)\text{H}$ channel, combinations of several triggers are used, all with the requirement that the missing transverse energy be above a given threshold. Extra requirements are added to keep the trigger rates low as the luminosity increases and to reduce the missing transverse energy thresholds in order to increase signal acceptance. A trigger with missing transverse energy > 150 GeV is used for the complete data set in both 2011 and 2012. During 2011 this trigger was used in conjunction with triggers that require the presence of two central jets ($|\eta| < 2.6$) with $p_\text{T} > 20$ GeV and missing transverse energy thresholds of 80 and 100 GeV, depending on the luminosity. During 2012 this trigger was used in conjunction with a trigger that required two central jets with $p_\text{T} > 30$ GeV and a missing transverse energy threshold of 80 GeV. This last trigger was discontinued when the instantaneous luminosity went above $3 \times 10^{33}\text{cm}^{-2}\text{s}^{-1}$ and was replaced by a trigger that requires missing transverse energy > 100 GeV, at least one pair of central jets with vectorial sum $p_\text{T} > 100$ GeV and individual p_T above 60 and 25 GeV respectively, and no jet with $p_\text{T} > 40$ GeV closer than 0.5 in azimuthal angle to the missing transverse energy direction. For $\text{Z}(\nu\nu)\text{H}$ events with missing transverse energy > 170 GeV, the combined trigger efficiency for $\text{Z}(\nu\nu)\text{H}$ signal events is $\approx 97\%$ with respect to the offline event reconstruction and selection, described below. For $\text{Z}(\nu\nu)\text{H}$ events with missing transverse energy between 130 and 170 GeV the corresponding efficiency is about 66%.

4 Event Reconstruction

The reconstructed interaction vertex with the largest value of $\sum_i p_{\mathrm{T}_i}^2$, where p_{T_i} is the transverse momentum of the i-th track associated with the vertex, is selected as the primary event vertex. This vertex is used as the reference vertex for all relevant objects in the event, which are reconstructed with the particle-flow algorithm. The pile-up interactions affect jet momentum reconstruction, missing transverse energy reconstruction, lepton isolation and b-tagging efficiency. To mitigate these effects, a track-based algorithm that filters all charged hadrons that do not originate from the primary interaction is used. In addition, a calorimeter-based algorithm evaluates the energy density in the calorimeter from interactions not related to the primary vertex and subtracts it from reconstructed jets in the event [22].

Jets are reconstructed from particle-flow objects using the anti-k_T clustering algorithm [23], as implemented in the FASTJET package [24, 25], with a distance parameter of 0.5. Each jet is required to lie within $|\eta| < 2.5$, to have at least two tracks associated to it, and to have electromagnetic and hadronic energy fractions of at least 1% of the total jet energy. Jet energy corrections, as a function of pseudorapidity and transverse momentum of the jet, are applied [26]. The missing transverse energy vector is calculated offline as the negative of the vectorial sum of transverse momenta of all particle-flow objects identified in the event, and the magnitude of this vector is referred to as $E_{\mathrm{T}}^{\mathrm{miss}}$ in the rest of this note.

Electron reconstruction requires the matching of an energy cluster in the ECAL with a track in the silicon tracker [27]. Identification criteria based on the ECAL shower shape, track-ECAL cluster matching, and consistency with the primary vertex are imposed. Additional requirements are imposed to remove electrons produced by photon conversions. In this analysis, electrons are considered in the pseudorapidity range $|\eta| < 2.5$, excluding the $1.44 < |\eta| < 1.57$ transition region between the ECAL barrel and endcap.

Muons are reconstructed using two algorithms [28]: one in which tracks in the silicon tracker are matched to signals in the muon chambers, and another in which a global track fit is performed seeded by signals in the muon system. The muon candidates used in the analysis are required to be reconstructed successfully by both algorithms. Further identification criteria are imposed on the muon candidates to reduce the fraction of tracks misidentified as muons. These include the number of measurements in the tracker and the muon system, the fit quality of the global muon track, and its consistency with the primary vertex. Muon candidates are considered in the $|\eta| < 2.4$ range.

Charged leptons from W and Z boson decays are expected to be isolated from other activity in the event. For each lepton candidate, a cone is constructed around the track direction at the event vertex. The scalar sum of the transverse momentum of each reconstructed particle compatible with the primary vertex and contained within the cone is calculated excluding the contribution from the lepton candidate itself. If this sum exceeds approximately 10% of the candidate p_{T}, the lepton is rejected; the exact requirement depends on the lepton η, p_{T} and its flavor.

The Combined Secondary Vertex (CSV) b-tagging algorithm [29] is used to identify jets that are likely to arise from the hadronization of b quarks. This algorithm combines in an optimal way the information about track impact parameters and secondary vertices within jets in a likelihood discriminant to provide separation of b jets from jets originating from light quarks, gluons and charm quarks. The efficiency to tag b jets and the rate of misidentification of non-b jets depend on the operating point chosen, and are typically parametrized as a function of the transverse momentum and pseudorapidity of the jets. These performance mea-

surements are obtained directly from data in samples that can be enriched in b jets, such as $\mathrm{t\bar{t}}$ and multi-jet events (where, for example, requiring the presence of a muon in the jets enhances its heavy-flavor content). Several working points for the CSV output discriminant (which can have values between zero and one) are used in the analysis. For a CSV > 0.90 requirement the efficiencies to tag b quarks, c quarks, and light quarks or gluons are approximately 50%, 6%, and 0.15%, respectively [30]. The corresponding efficiencies for CSV > 0.50 are approximately 72%, 23%, and 3%.

All events from data and from the simulated samples are required to pass the same triggers and event reconstruction algorithms. Scale factors that account for the differences in the performance of these algorithms between data and simulations are computed and used in the analysis.

5 Event Selection

The background processes to VH production are vector-boson+jets (V+jets), $\mathrm{t\bar{t}}$, single-top, dibosons (VV) and QCD multijet production. These overwhelm the signal by several orders of magnitude. The event selection is based first on the kinematic reconstruction of the vector bosons and the Higgs boson decay into two b-tagged jets. Backgrounds are then substantially reduced by requiring a significant boost of the p_{T} of the vector boson and the Higgs boson [31], which tend to recoil away from each other with a large azimuthal opening angle, $\Delta\phi(\mathrm{V},\mathrm{H})$, between them. For each mode two regions of $p_{\mathrm{T}}(\mathrm{V})$ boost are considered. These are referred to as "low" and "high" in the rest of the document. Due to different signal and background composition, each boost region has different sensitivity and the analysis is performed separately in each region. The results from both regions are then combined for each mode. The boost regions for the $\mathrm{W}(\ell\nu)\mathrm{H}$ channels are $120 < p_{\mathrm{T}}(\mathrm{V}) < 170$ GeV and $p_{\mathrm{T}}(\mathrm{V}) > 170$ GeV; for the $\mathrm{Z}(\nu\nu)\mathrm{H}$ channel the regions are $130 < p_{\mathrm{T}}(\mathrm{V}) < 170$ GeV and $p_{\mathrm{T}}(\mathrm{V}) > 170$ GeV; and for the $\mathrm{Z}(\ell\ell)\mathrm{H}$ channels, $50 < p_{\mathrm{T}}(\mathrm{V}) < 100$ GeV and $p_{\mathrm{T}}(\mathrm{V}) > 100$ GeV.

Candidate $\mathrm{W} \to \ell\nu$ decays are identified by requiring the presence of a single isolated lepton and additional missing transverse energy. Muons are required to have a p_{T} above 20 GeV; the corresponding value for electrons is 30 GeV. For the $\mathrm{W}(\mathrm{e}\nu)\mathrm{H}$ analysis, $E_{\mathrm{T}}^{\mathrm{miss}}$ is required to be greater than 45 GeV to reduce contamination from QCD multijet processes. Candidate $\mathrm{Z} \to \ell\ell$ decays are reconstructed by combining isolated, oppositely charged pairs of electrons or muons and requiring the dilepton invariant mass to satisfy $75 < m_{\ell\ell} < 105$ GeV. For Z candidates the lepton p_{T} is required to be greater than 20 GeV. The identification of $\mathrm{Z} \to \nu\bar{\nu}$ decays requires the $E_{\mathrm{T}}^{\mathrm{miss}}$ in the event to be within the $p_{\mathrm{T}}(\mathrm{V})$ regions described above. The QCD multijet background is reduced to negligible levels in this channel when requiring that the $E_{\mathrm{T}}^{\mathrm{miss}}$ does not originate from mismeasured jets. To that end two event requirements are made. First, a $\Delta\phi(\mathrm{E}_{\mathrm{T}}^{\mathrm{miss}},\mathrm{jet}) > 0.5$ radians requirement is applied on the azimuthal angle between the $E_{\mathrm{T}}^{\mathrm{miss}}$ direction and the closest jet with $|\eta| < 2.5$ and $p_{\mathrm{T}} > 20$ GeV for the 7 TeV analysis or $p_{\mathrm{T}} > 30$ GeV for the 8 TeV analysis (where more pile-up is present). The second requirement is that the azimuthal angle between the missing transverse energy as calculated from charged tracks only (with $p_{\mathrm{T}} > 0.5$ GeV and $|\eta| < 2.5$) and the $E_{\mathrm{T}}^{\mathrm{miss}}$, $\Delta\phi(\mathrm{E}_{\mathrm{T}}^{\mathrm{miss}},\mathrm{E}_{\mathrm{T}}^{\mathrm{miss}(\mathrm{trks})})$, should be smaller than 0.5 radians. To reduce backgrounds from $\mathrm{t\bar{t}}$ and WZ in the $\mathrm{W}(\ell\nu)\mathrm{H}$ and $\mathrm{Z}(\nu\nu)\mathrm{H}$ channels, events with additional isolated leptons, N_{al}, with $p_{\mathrm{T}} > 20$ GeV are rejected.

The reconstruction of the $\mathrm{H} \to \mathrm{b\bar{b}}$ decay is made by requiring the presence of two central ($|\eta| < 2.5$) jets above a minimum p_{T} threshold, and tagged by the CSV algorithm, requiring that the value of the CSV discriminator be above a certain threshold. If more than two such jets are

found in the event, the pair of jets with the highest vectorial sum of transverse momenta, $p_T(jj)$, is selected. After the b-tagging requirements are applied, the fraction of $H \to b\bar{b}$ candidates in signal events that contain the two b jets from the Higgs boson decay is near 100%. The background from V+jets and dibosons is reduced significantly through b tagging, and subprocesses where the two jets originate from genuine b quarks dominate the final selected data sample. After all event selection criteria described in this Section are applied, the dijet invariant mass resolution of the two b jets from the Higgs decay is approximately 10%, with a few percent bias on the mass. To increase the sensitivity of the analysis with respect to [12], a new category of events is added in the high $p_T(V)$ regions of the $W(\ell\nu)H$ and $Z(\nu\nu)H$ channels, in which the value of the CSV discriminator for the b-tagged jet with the second largest CSV value is required to be looser.

The Higgs boson mass resolution is improved by applying regression techniques similar to those used at the CDF experiment [32]. A further correction, beyond the standard CMS jet energy corrections, is computed for individual b jets in an attempt to recalibrate to the true parton energy. For this purpose, a specialized BDT algorithm is trained on simulated $H \to b\bar{b}$ signal events with inputs that include detailed information about the jet structure and that help differentiate jets from b quarks from light-flavor jets. These include variables containing information about several properties of a secondary vertex (when present), information about tracks, jet constituents, and other variables related to the energy reconstruction of the jet. In the cases where a soft lepton is found in or nearby the jet, the p_T of the lepton, the distance between the lepton and the jet and the momentum of the lepton transverse to the jet direction are also included in the BDT regression. The improvement on the mass resolution is approximately 15%, resulting in an increase in the analysis sensitivity of 10–20%, depending on the specific channel. This BDT regression is implemented in the TMVA framework [33].

In the final stage of the analysis, to better separate signal from background under different Higgs boson mass hypotheses, another BDT algorithm is trained separately at each mass value using simulated samples for signal and background that pass the event selection described above. The set of input variables used is chosen by iterative optimization from a larger number of potentially discriminating variables. Table 1 lists these variables. Jets are counted as additional jets if they satisfy the following: $p_T > 20$ GeV and $|\eta| < 4.5$ for $W(\ell\nu)H$, $p_T > 20$ GeV and $|\eta| < 2.5$ for $Z(\ell\ell)H$, and $p_T > 30$ GeV and $|\eta| < 4.5$ for $Z(\nu\nu)H$.

The event selection requirements that are applied on all samples before training are listed in Table 2. The shape of the output distribution of this BDT algorithm is the final discriminant on which a fit is performed to search for events resulting from Higgs boson production. Fitting this shape, rather than simply counting events in the region with better signal to background ratio as in [34], improves the sensitivity of the analysis by approximately 20%.

6 Background Control Regions

Appropriate control regions are identified in data and used to correct the Monte Carlo yield estimates for several of the most important background processes: production of W and Z bosons in association with jets (light- and heavy-flavor) and $t\bar{t}$ production. A set of simultaneous fits is then performed to the distributions of discriminating variables in the control regions, separately in each channel, to obtain consistent scale factors by which the Monte Carlo yields are adjusted. These scale factors account not only for cross section discrepancies, but also potential residual differences in physics object selection. Therefore, separate scale factors are used for each background process in the different channels. The uncertainties in the scale factor determination include a statistical uncertainty coming from the fits (affected by the finite size of the

Table 1: Variables used in the BDT training.

Variable
$p_{\mathrm{T}j}$: transverse momentum of each Higgs daughter
$m(\mathrm{jj})$: dijet invariant mass
$p_{\mathrm{T}}(\mathrm{jj})$: dijet transverse momentum
$p_{\mathrm{T}}(\mathrm{V})$: vector boson transverse momentum (or $E_{\mathrm{T}}^{\mathrm{miss}}$)
$\mathrm{CSV}_{\mathrm{max}}$: value of CSV for the Higgs daughter with largest CSV value
$\mathrm{CSV}_{\mathrm{min}}$: value of CSV for the Higgs daughter with second largest CSV value
$\Delta\phi(\mathrm{V},\mathrm{H})$: azimuthal angle between V (or $E_{\mathrm{T}}^{\mathrm{miss}}$) and dijet
$\lvert\Delta\eta(\mathrm{jj})\rvert$: difference in η between Higgs daughters
$\Delta R(\mathrm{jj})$: distance in η–ϕ between Higgs daughters
N_{aj}: number of additional jets
$\Delta\phi(\mathrm{E}_{\mathrm{T}}^{\mathrm{miss}},\mathrm{jet})$: azimuthal angle between $E_{\mathrm{T}}^{\mathrm{miss}}$ and the closest jet (only for $\mathrm{Z}(\nu\nu)\mathrm{H}$)
$\Delta\theta_{\mathrm{pull}}$: color pull angle [35]

Table 2: Selection criteria for the samples used in the BDT training in each channel. Entries marked with "–" indicate that the variable is not used in the given channel. Entries in parenthesis indicate the selection for the high $p_{\mathrm{T}}(\mathrm{V})$ region. The second and third rows refer to the p_{T} thresholds on the leading (j_1) and sub-leading (j_2) jets. $\mathrm{CSV}_{\mathrm{min}}^{loose}$ is the requirement for the loose b-tag category. The values listed for kinematical variables are in units of GeV.

Variable	$\mathrm{W}(\ell\nu)\mathrm{H}$	$\mathrm{Z}(\ell\ell)\mathrm{H}$	$\mathrm{Z}(\nu\nu)\mathrm{H}$
$m_{\ell\ell}$	–	$[75-105]$	–
$p_{\mathrm{T}}(j_1)$	>30	>20	>60
$p_{\mathrm{T}}(j_2)$	>30	>20	>30
$p_{\mathrm{T}}(\mathrm{jj})$	>120	–	>130
$m(\mathrm{jj})$	<250	$[80-150]$ (<250)	<250
$p_{\mathrm{T}}(\mathrm{V})$	$[120-170]$ (>170)	$[50-100]$ (>100)	–
$\mathrm{CSV}_{\mathrm{max}}$	>0.40	>0.50 (>0.244)	>0.679
$\mathrm{CSV}_{\mathrm{min}}$	>0.40	>0.244	>0.244
$\mathrm{CSV}_{\mathrm{min}}^{loose}$	– (<0.40)	–	– (<0.244)
N_{al}	$=0$	–	$=0$
$E_{\mathrm{T}}^{\mathrm{miss}}$	>45 (elec)	–	$[130-170]$ (>170)
$\Delta\phi(\mathrm{E}_{\mathrm{T}}^{\mathrm{miss}},\mathrm{jet})$	–	–	>0.5
$\Delta\phi(\mathrm{E}_{\mathrm{T}}^{\mathrm{miss}},\mathrm{E}_{\mathrm{T}}^{\mathrm{miss}(\mathrm{trks})})$	–	–	<0.5
$\Delta\phi(\mathrm{V},\mathrm{H})$	–	–	>2.0

Table 3: Definition of control regions for the Z($\ell\ell$)H channel. The same selection is used for both the low and high $p_T(V)$ regions. The values listed for kinematical variables are in units of GeV.

Variable	Z+jets	$t\bar{t}$
$m_{\ell\ell}$	$[75-105]$	veto $[75-105]$
$p_T(j_1)$	>20	>20
$p_T(j_2)$	>20	>20
$p_T(V)$	$[50-100]$	$[50-100]$
CSV_{max}	>0.244	>0.244
CSV_{min}	>0.244	>0.244
$m(jj)$	veto $[80-150]$, <250	veto $[80-150]$, <250

Table 4: Definition of control regions for the Z($\nu\nu$)H channel for the low and high $p_T(V)$ regions. The values in parenthesis are used for the high $p_T(V)$ region. LF and HF refer to light- and heavy-flavor jets. N_{al} is the number of additional isolated leptons in the event. The values listed for kinematical variables are in units of GeV.

Variable	Z+LF	Z+HF	$t\bar{t}$	W+LF	W+HF
$p_T(j_1)$	>60	>60	>60	>60	>60
$p_T(j_2)$	>30	>30	>30	>30	>30
$p_T(jj)$	>130	>130	>130	>130	>130
$p_T(V)$	–	–	–	–	–
CSV_{max}	$[0.244-0.898]$	>0.679	>0.898	$[0.244-0.898]$	>0.679
CSV_{min}	–	>0.244	–	–	>0.244
N_{aj}	–	–	≥ 1	$=0$	$=0$
N_{al}	$=0$	$=0$	$=1$	$=1$	$=1$
E_T^{miss}	$[130-170](>170)$	$[130-170](>170)$	$[130-170](>170)$	$[130-170](>170)$	$[130-170](>170)$
$\Delta\phi(E_T^{miss}, jet)$	>0.5	>0.5	>0.5	>0.5	>0.5
$\Delta\phi(E_T^{miss}, E_T^{miss(trks)})$	<0.5	<0.5	–	–	–
$m(jj)$	<250	veto $[100-140]$	veto $[100-140]$	<250	veto $[100-140]$

samples) and an associated systematic uncertainty obtained by refitting the distributions in the control regions when modified by the uncertainty of various sources of systematic uncertainty such as b-tagging, jet energy scale, and jet energy resolution.

Tables 3–5 list the selection criteria used for the control regions for the Z($\ell\ell$)H, Z($\nu\nu$)H and W($\ell\nu$)H channels, respectively. Table 6 summarizes the fit results for all channels for the 7 TeV and 8 TeV data, respectively. In general, the fit results are very good and reliable scale factors are determined that are consistent with estimates from the previous version of this analysis [34].

7 Uncertainties

The primary result described in this note is an upper limit on the production of a standard model Higgs boson produced in association with a vector boson and decaying to a $b\bar{b}$ pair. Uncertainties on the expected signal and background yields and shapes affect the upper limit. Table 7 lists the uncertainties considered that enter in the limit calculation.

The uncertainty in the CMS luminosity measurement for the data set used in the analysis is estimated to be 2.2% for the 2011 data [36] and 4.4% for the 2012 data [37]. Muon and electron trigger, reconstruction, and identification efficiencies are determined in data from samples of

Table 5: Definition of control regions for the W($\ell\nu$)H channels for the low and high p_T(V) regions. The values in parenthesis are used for the high p_T(V) region. LF and HF refer to light- and heavy-flavor jets. N_{al} is the number of additional isolated leptons in the event. METsig is the significance of the E_T^{miss}. The values listed for kinematical variables are in units of GeV.

Variable	W+LF	$t\bar{t}$	W+HF
$p_T(j_1)$	> 30	> 30	> 30
$p_T(j_2)$	> 30	> 30	> 30
$p_T(jj)$	> 120	> 120	> 120
$p_T(V)$	$[120 - 170]$ (> 170)	$[120 - 170]$ (> 170)	$[120 - 170]$ (> 170)
CSV_{max}	$[0.244 - 0.898]$	> 0.898	> 0.898
N_{aj}	< 2	> 1	$= 0$
N_{al}	$= 0$	$= 0$	$= 0$
E_T^{miss}	> 35 (e only)	> 35 (e only)	> 45 (e only)
METsig	$> 2.0(\mu)$ $> 3.0(e)$	–	–
$m(jj)$	< 250	< 250	veto $[90 - 150]$

Table 6: Data/MC scale factors for each control region in each decay mode for the 2011 7 TeV and the 2012 8 TeV analyses. The errors include the statistical uncertainty from the fit, and a systematic uncertainty accounting for possible data/MC shape differences in the discriminating variables. Electron and muon samples in Z($\ell\ell$)H and W($\ell\nu$)H are fit simultaneously to determine average scale factors.

Process	W($\ell\nu$)H	W($\ell\nu$)H	Z($\ell\ell$)H	Z($\ell\ell$)H	Z($\nu\nu$)H	Z($\nu\nu$)H
Low p_T	7 TeV	8 TeV	7 TeV	8 TeV	7 TeV	8 TeV
W + udscg	$0.88 \pm 0.01 \pm 0.03$	$1.01 \pm 0.02 \pm 0.01$	–	–	$0.89 \pm 0.01 \pm 0.03$	$0.96 \pm 0.06 \pm 0.03$
W$b\bar{b}$	$1.91 \pm 0.14 \pm 0.31$	$2.07 \pm 0.15 \pm 0.10$	–	–	$1.36 \pm 0.10 \pm 0.15$	$1.30 \pm 0.17 \pm 0.10$
Z + udscg	–	–	$1.11 \pm 0.03 \pm 0.11$	$1.10 \pm 0.02 \pm 0.06$	$0.87 \pm 0.01 \pm 0.03$	$1.15 \pm 0.07 \pm 0.03$
Z$b\bar{b}$	–	–	$0.98 \pm 0.05 \pm 0.12$	$1.08 \pm 0.04 \pm 0.08$	$0.96 \pm 0.02 \pm 0.03$	$1.12 \pm 0.10 \pm 0.04$
$t\bar{t}$	$0.93 \pm 0.02 \pm 0.05$	$1.07 \pm 0.01 \pm 0.01$	$1.03 \pm 0.04 \pm 0.11$	$1.01 \pm 0.02 \pm 0.06$	$0.97 \pm 0.02 \pm 0.04$	$1.05 \pm 0.07 \pm 0.03$
High p_T	7 TeV	8 TeV	7 TeV	8 TeV	7 TeV	8 TeV
W + udscg	$0.79 \pm 0.01 \pm 0.02$	$0.94 \pm 0.02 \pm 0.01$	–	–	$0.78 \pm 0.02 \pm 0.03$	$0.95 \pm 0.05 \pm 0.02$
W$b\bar{b}$	$1.49 \pm 0.14 \pm 0.19$	$1.72 \pm 0.16 \pm 0.08$	–	–	$1.48 \pm 0.15 \pm 0.20$	$1.27 \pm 0.18 \pm 0.10$
Z + udscg	–	–	$1.11 \pm 0.03 \pm 0.11$	$1.10 \pm 0.02 \pm 0.06$	$0.97 \pm 0.02 \pm 0.04$	$1.04 \pm 0.07 \pm 0.02$
Z$b\bar{b}$	–	–	$0.98 \pm 0.05 \pm 0.12$	$1.08 \pm 0.04 \pm 0.08$	$1.08 \pm 0.09 \pm 0.06$	$1.15 \pm 0.10 \pm 0.04$
$t\bar{t}$	$0.84 \pm 0.02 \pm 0.03$	$0.99 \pm 0.01 \pm 0.01$	$1.03 \pm 0.04 \pm 0.11$	$1.01 \pm 0.02 \pm 0.06$	$0.97 \pm 0.02 \pm 0.04$	$1.03 \pm 0.07 \pm 0.03$

leptonic Z boson decays. The uncertainty on the yields due to the trigger efficiency is 2% per charged lepton and the uncertainty on the identification efficiency is also 2% per lepton. The parameters describing the $Z(\nu\nu)H$ trigger efficiency turn-on curve have been varied within their statistical uncertainties and for different assumptions on the methodology to derive the efficiency. A yield uncertainty of about 3% is estimated.

The jet energy scale is varied within one standard deviation as a function of jet p_T and η. The efficiency of the analysis selection is recomputed to assess the variation in yield. Depending on the process, a 2–3% yield variation is found. The effect of the uncertainty on the jet energy resolution is evaluated by smearing the jet energies according to the measured uncertainty. Depending on the process, a 3–6% variation in yields due to this effect is obtained. The uncertainties in the jet energy scale and resolution also have an effect on the shape of the BDT output distribution. The impact of the jet energy scale uncertainty is determined by recomputing the BDT distribution after shifting the energy scale up and down by its uncertainty. Similarly, the impact of the jet energy resolution is determined by recomputing the BDT distribution after increasing or decreasing the jet energy resolution. An uncertainty of 3% is assigned to the yields of all processes in the $W(\ell\nu)H$ and $Z(\nu\nu)H$ modes due to the uncertainty related to the missing transverse energy estimate.

Data-to-simulation b-tagging scale factors, measured in $t\bar{t}$ events, are applied consistently to jets in signal and background events. The measured uncertainties for the b-tagging scale factors are: 6% per b tag, 12% per charm tag, and 15% per mistagged jet (originating from gluons and light u, d, s quarks) [29]. These translate into yield uncertainties in the 3–15% range, depending on the channel and the specific process. The shape of the BDT output distribution is also affected by the shape of the CSV distribution and therefore recomputed according to an up and down range of variations of the CSV distributions.

The total VH signal cross section has been calculated to next-to-next-to-leading order (NNLO) accuracy, and the total theoretical uncertainty is 4% [38], including the effect of scale and PDF variations [39–43]. This analysis is performed in the boosted regime, and thus, potential differences in the p_T spectrum of the V and H between data and Monte Carlo simulations could introduce systematic effects in the signal acceptance and efficiency estimates. Two calculations are available that estimate the next-to-leading-order (NLO) electroweak [44–46] and NNLO QCD [47] corrections to VH production in the boosted regime. The estimated effect due to electroweak corrections for a boost of ~ 150 GeV is 5% for ZH and 10% for WH. For the QCD correction, a 10% uncertainty is estimated for both ZH and WH, which includes effects due to additional jet activity from initial- and final-state radiations. The finite size of the signal Monte Carlo samples, after all selection criteria are applied, contributes 1–5% uncertainty across all channels.

The uncertainty in the background yields that results from the estimates from data is approximately 10%. For V+jets we consider the differences in shape of the BDT output distribution for events from the MADGRAPH and HERWIG++ Monte Carlo generators. Uncertainties of 15% and 30% are assigned to the yields obtained from simulation for single-top production in the t-channel and in the tW-channel, respectively. These uncertainties are extracted from the CMS measurements in [48]. For the diboson backgrounds, a 30% cross section uncertainty is assumed.

Table 7: Uncertainties in the signal and background yields due to the systematic uncertainty in the sources listed. The ranges quoted are due to variations from 7 to 8 TeV data, different modes, specific processes, and Higgs boson mass hypothesis. See text for details.

Source	Range
Luminosity	2.2-4.4%
Lepton efficiency and trigger (per lepton)	3%
$Z(\nu\nu)H$ triggers	3%
Jet energy scale	2–3%
Jet energy resolution	3–6%
Missing transverse energy	3%
b-tagging	3–15%
Signal cross section (scale and PDF)	4%
Signal cross section (p_T boost, EWK/QCD)	5–10% / 10%
Signal Monte Carlo statistics	1-5%
Backgrounds (data estimate)	$\approx$ 10%
Single-top (simulation estimate)	15–30%
Dibosons (simulation estimate)	30%

8 Results

The results are obtained from combined signal and background fits to the shape of the output distributions of the BDT algorithms trained separately for each channel and for each Higgs boson mass hypothesis in the 110–135 GeV range examined. In the fit the BDT shape and normalization, for signal and for each background component, are allowed to vary within the systematic and statistical uncertainties described in Section 7. These uncertainties are treated as nuisance parameters in the fit, with appropriate correlations taken into account. All nuisance parameters, including the scale factors described in Section 6 get adjusted by the fit. Figs. 1–5 show examples of these BDT distributions, using the adjusted scale factors, for the m_H= 125 GeV training for both $p_T(V)$ bins, each channel, for the 8 TeV data.

The results of all channels, for the two $p_T(V)$ bins and for both the 7 TeV and the 8 TeV data, are combined to obtain 95% confidence level upper limits on the product of the VH production cross section times the $H \to b\bar{b}$ branching ratio, with respect to the expectations for a standard model Higgs boson (σ/σ_{SM}). The observed limits at each mass point, the median expected limits, and the 1σ and 2σ bands are calculated using the modified frequentist method CL_s [49–51]. Table 8 lists these limits, and Fig. 6 displays the results. In the mass range studied, the observed 95% CL upper limits vary from 1.0 to 4.2 times the standard model prediction, and the corresponding expected limits vary from 0.9 to 1.9. At a Higgs boson mass of 125 GeV the observed limit is 2.5 and the expected limit is 1.2. The maximum excess is observed near a Higgs boson mass of 130 GeV. Given that the resolution for the reconstructed Higgs boson mass is $\approx$ 10%, the results are very compatible with a Higgs mass of 125 GeV. This is demonstrated by the red dashed line in the figure, which is the the observed limits obtained from replacing the data with the sum of expected background and signal for a Higgs boson at a mass of 125 GeV.

For all channels an excess of events over the expected background contributions is indicated by the fits of the BDT output distributions. Fig. 7 shows the probabilities (p-values) that the observed excess is due to background fluctuations alone, as a function of the Higgs boson mass hypothesis. For a mass of 125 GeV the excess of observed events is 2.2 standard deviations, and is consistent with the standard model prediction for Higgs boson production. The fit also returns the most likely value of the production cross section for a 125 GeV Higgs boson, relative

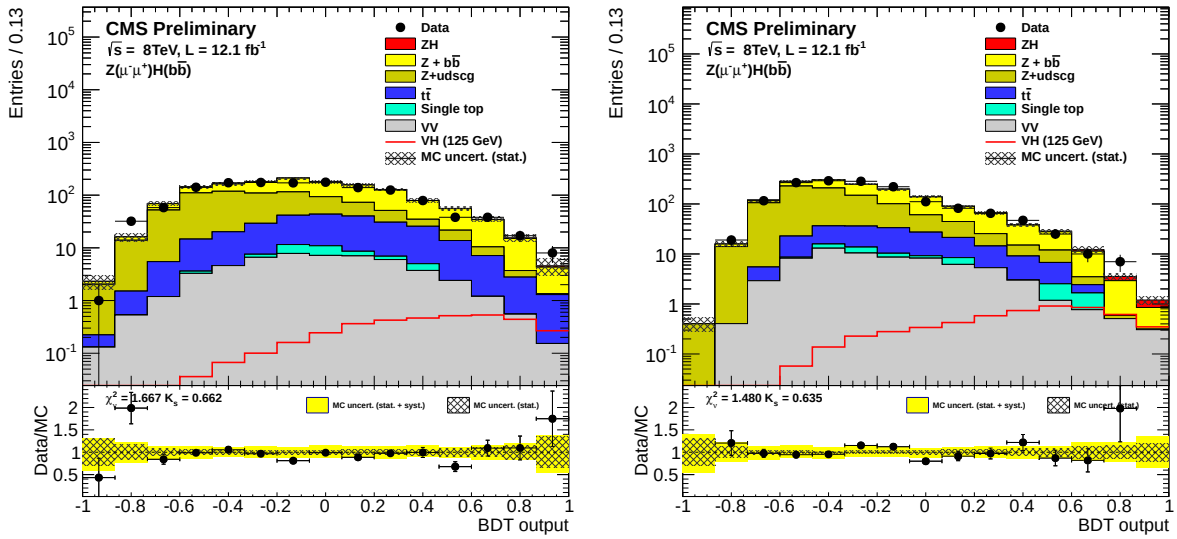

Figure 1: 8 TeV analysis. BDT output distributions for $Z(\mu\mu)H$ in the low $p_T(V)$ bin (left) and high $p_T(V)$ bin (right), for data (points with errors), all backgrounds, and signal, after all selection criteria have been applied.

to the standard model cross section (signal strength), for each mode and for all modes combined. These are also shown in Fig. 7. The observed signal strengths for the individual modes are consistent with each other and the value for the signal strength for all modes combined is $1.3^{+0.7}_{-0.6}$.

Fig. 8 shows the distribution of dijet invariant mass for the combination of all five channels in the combined 7 TeV and 8 TeV data using an event selection, described in Ref. [52]. This selection is more restrictive than the one used in the BDT analysis and that is optimized for a counting experiment in this observable. Fig. 8 also shows the same dijet invariant mass distribution with all backgrounds, except dibosons, subtracted. The data are consistent with the presence of a diboson signal, with a rate approximately as expected from the standard model, together with a small excess consistent with originating from the production of a 125 GeV standard model Higgs boson.

9 Conclusions

A search for the standard model Higgs boson decaying to $b\bar{b}$ when produced in association with a weak vector boson is reported for the $W(\mu\nu)H$, $W(e\nu)H$, $Z(\mu\mu)H$, $Z(ee)H$ and $Z(\nu\nu)H$ channels. The search is performed in data samples corresponding to integrated luminosities of 5.0 fb^{-1} at $\sqrt{s} = 7$ TeV and 12.1 fb^{-1} at $\sqrt{s} = 8$ TeV, recorded by the CMS experiment at the LHC. Upper limits, at the 95% confidence level, on the VH production cross section times the $H \to b\bar{b}$ branching ratio, with respect to the expectations for a standard model Higgs boson, are derived for a Higgs boson in the mass range 110–135 GeV. In this range, the observed upper limits vary from 1.0 to 4.2 times the standard model prediction; the corresponding expected limits vary from 0.9 to 1.9. At a Higgs boson mass of 125 GeV the observed limit is 2.5 and the expected limit is 1.2. An excess of events is observed above the expected background with a local significance of 2.2 standard deviations, which is consistent with the expectation from the production of the standard model Higgs boson.

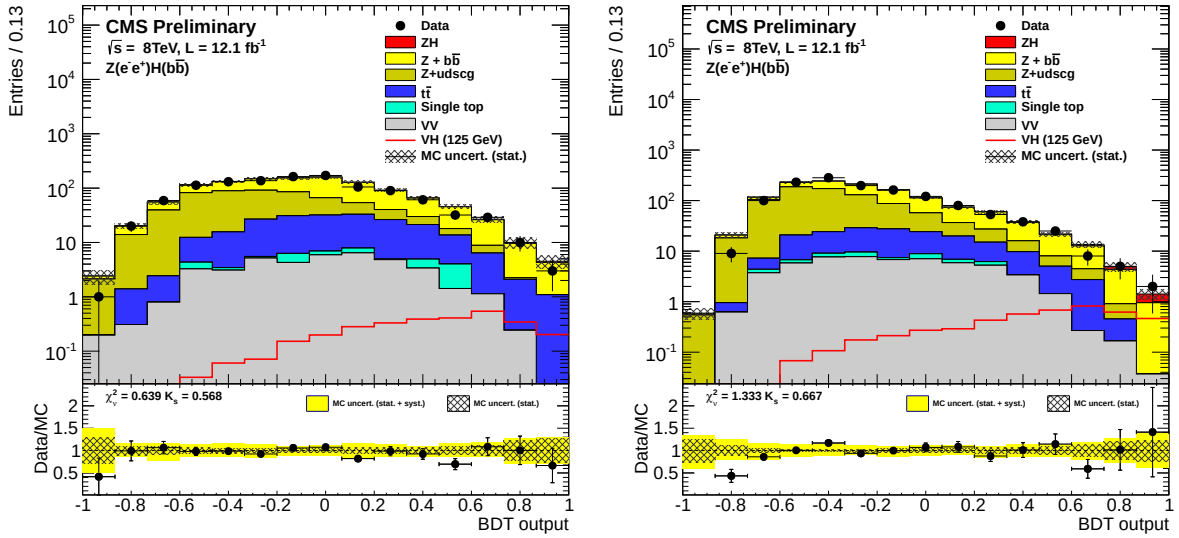

Figure 2: 8 TeV analysis. BDT output distributions for Z(ee)H in the low $p_{\mathrm{T}}(\mathrm{V})$ bin (left) and high $p_{\mathrm{T}}(\mathrm{V})$ bin (right), for data (points with errors), all backgrounds, and signal, after all selection criteria have been applied.

Table 8: Expected and observed 95% CL upper limits on the product of the VH production cross section times the $\mathrm{H} \to \mathrm{b\bar{b}}$ branching ratio, with respect to the expectations for a standard model Higgs boson.

m_{H}(GeV)	110	115	120	125	130	135
Exp.	0.89	0.91	1.00	1.15	1.39	1.85
Obs.	0.99	1.60	1.64	2.45	3.40	4.19

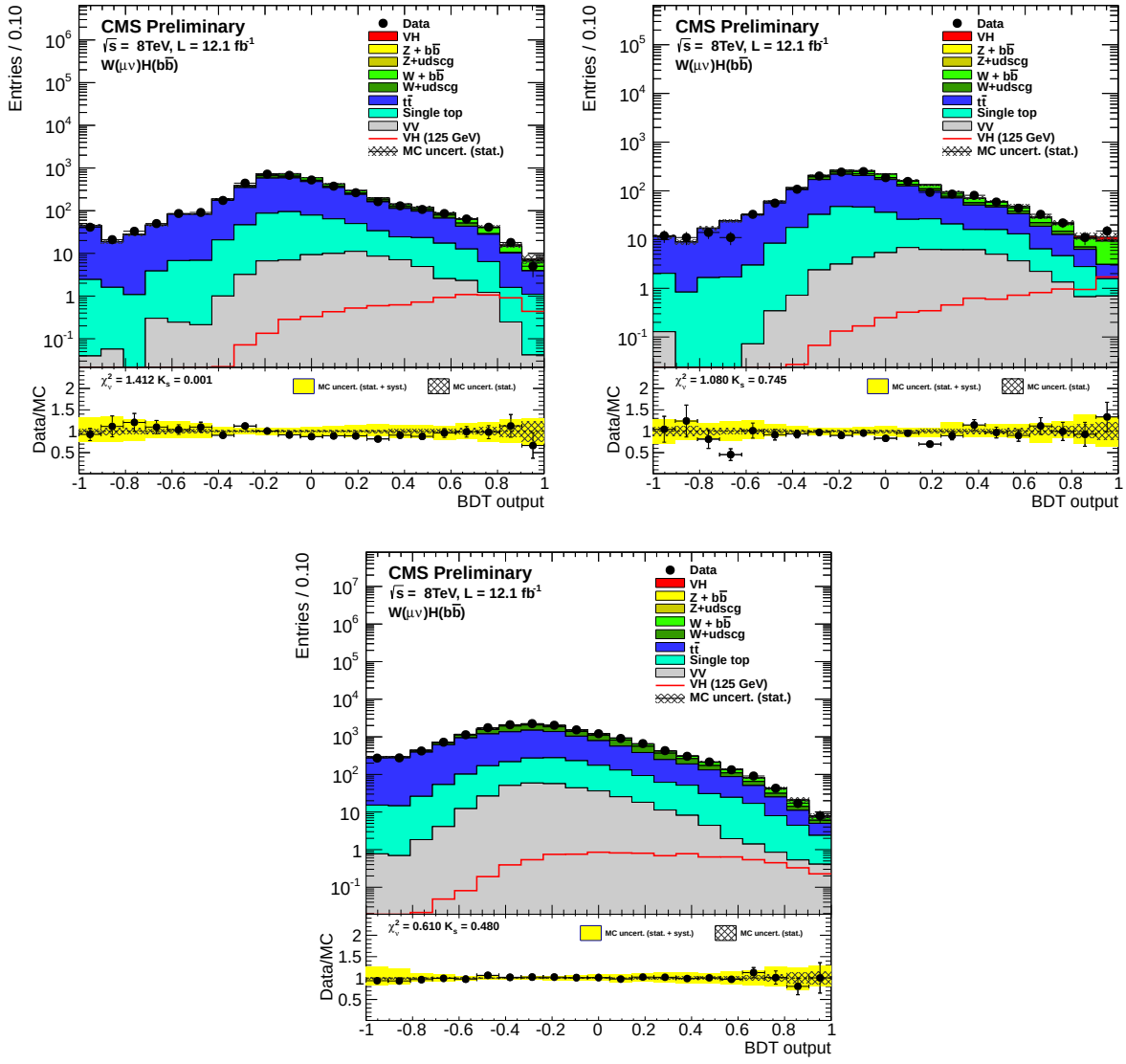

Figure 3: 8 TeV analysis. BDT output distributions for W($\mu\nu$)H in the low $p_{\mathrm{T}}(\mathrm{V})$ bin (left), high $p_{\mathrm{T}}(\mathrm{V})$ bin (right), and high $p_{\mathrm{T}}(\mathrm{V})$ bin with looser b-tagging (bottom), for data (points with errors), all backgrounds, and signal, after all selection criteria have been applied.

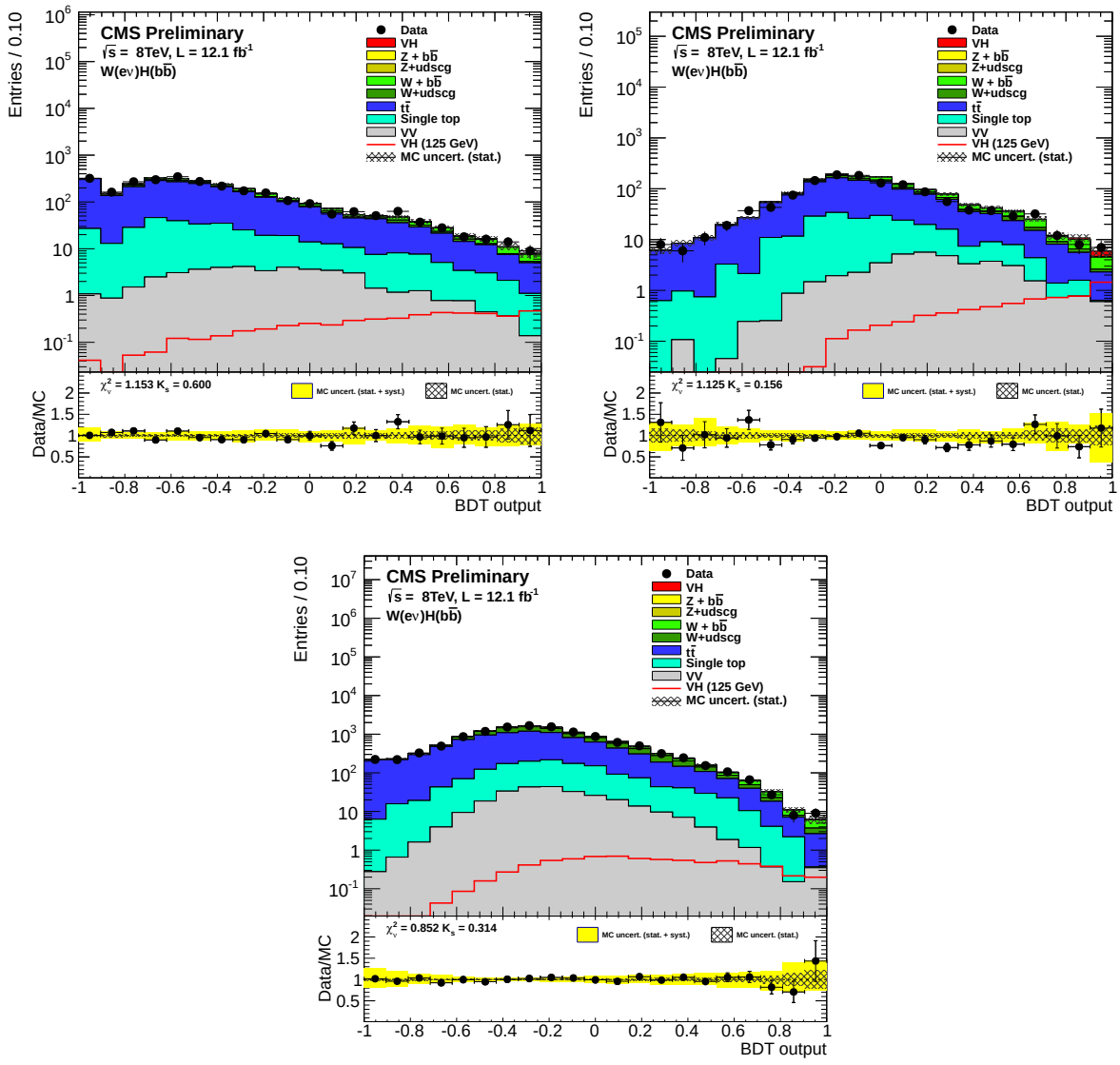

Figure 4: 8 TeV analysis. BDT output distributions for W($e\nu$)H in the low $p_{\mathrm{T}}(\mathrm{V})$ bin (left), high $p_{\mathrm{T}}(\mathrm{V})$ bin (right), and high $p_{\mathrm{T}}(\mathrm{V})$ bin with looser b-tagging (bottom), for data (points with errors), all backgrounds, and signal, after all selection criteria have been applied.

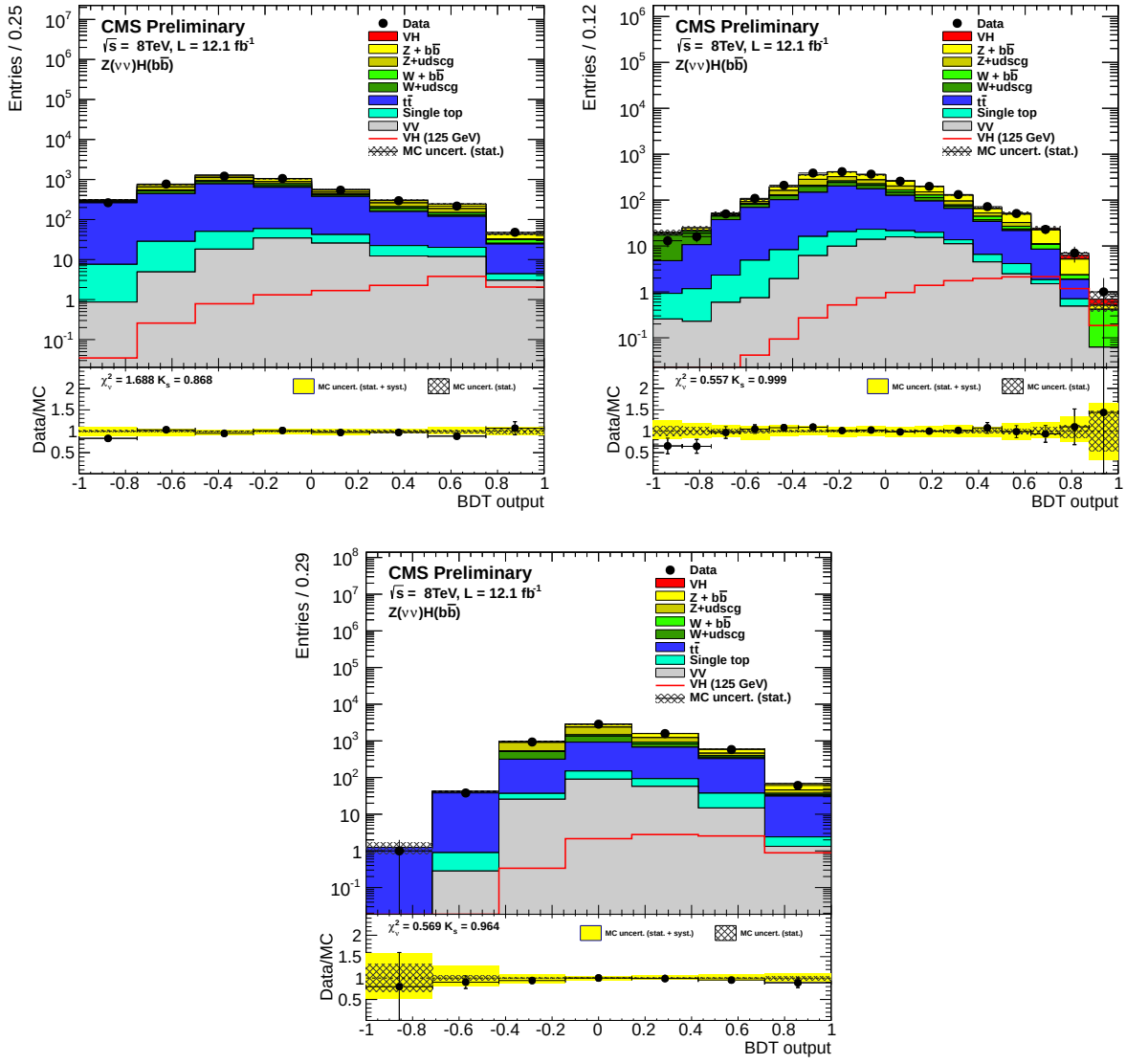

Figure 5: 8 TeV analysis. BDT output distributions for $Z(\nu\nu)H$ in the low $p_T(V)$ bin (left), the high $p_T(V)$ (right), and the high $p_T(V)$ with looser b-tagging (bottom), for data (points with errors), all backgrounds, and signal, after all selection criteria have been applied.

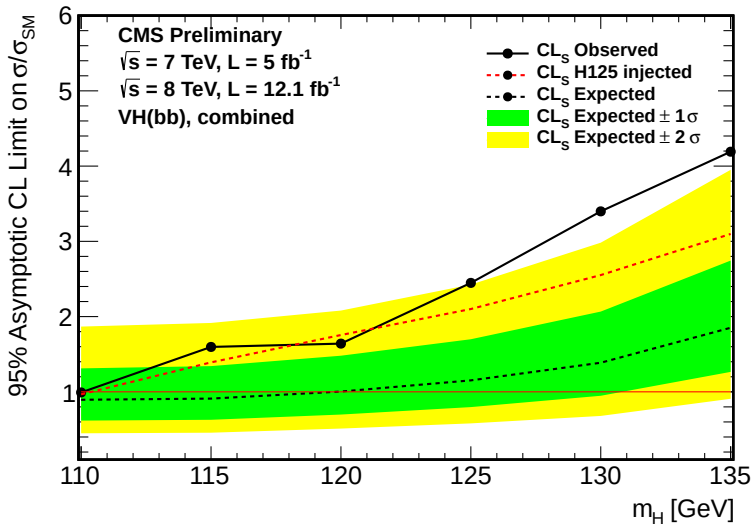

Figure 6: Expected and observed 95% CL upper limits on the product of the VH production cross section times the $H \to b\bar{b}$ branching ratio, with respect to the expectations for a standard model Higgs boson. The median expected limit and the 1- and 2-σ bands are obtained with the LHC CLs method as implemented in RooStats, as are the observed limits at each mass point. The limits are combined for the 2011 7 TeV and the 2012 8 TeV data.

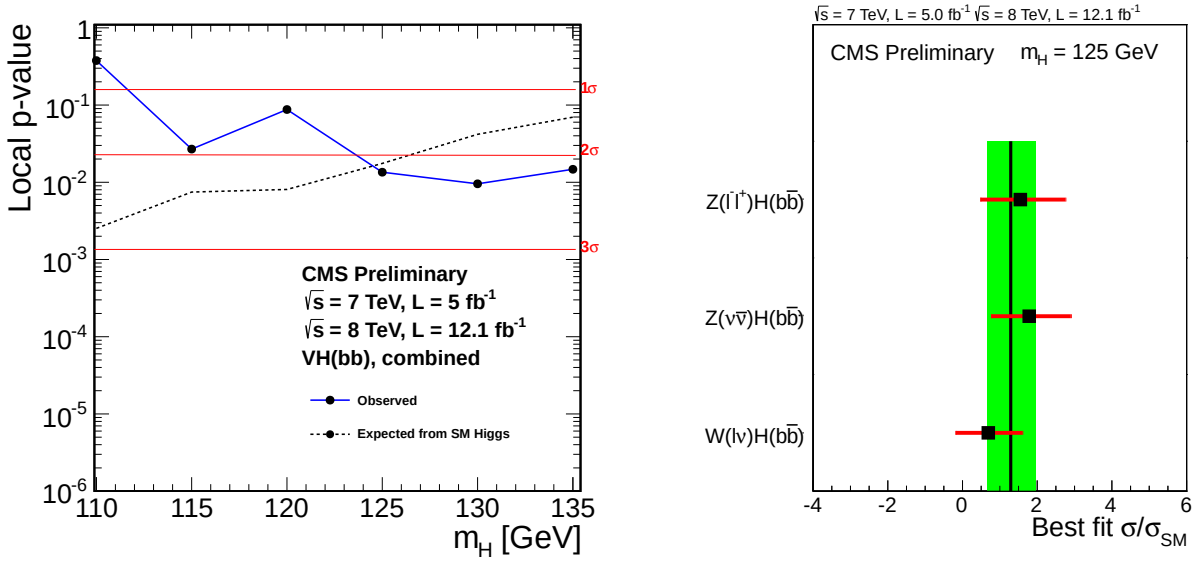

Figure 7: Left: p-values for background fluctuations to account for the observed excess of events in the data. Right: the most likely value of the production cross section for a 125 GeV Higgs boson, relative to the standard model cross section, for each mode and for all modes combined.

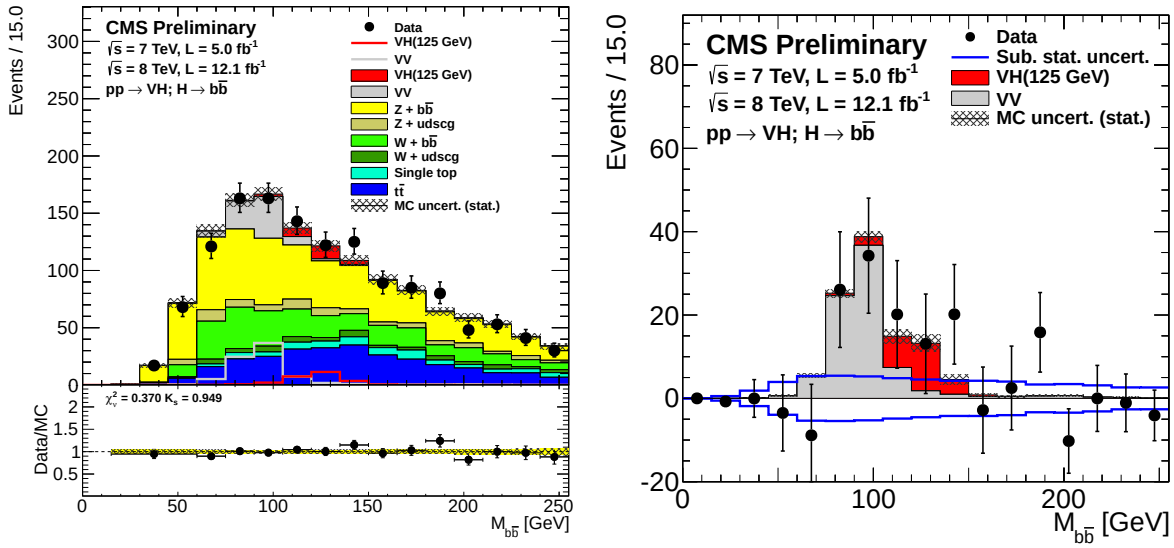

Figure 8: Left: dijet invariant mass distribution, combined for all channels, for the high $p_{\mathrm{T}}(\mathrm{V})$ bin, for events that pass an event selection optimized for this variable. Right: same distribution with all backgrounds, except dibosons, subtracted. The solid histograms for the backgrounds and the signal are summed cumulatively. The line histogram for signal and for VV backgrounds are also shown superimposed. The data is represented by points with error bars.

References

[1] ATLAS Collaboration, "Observation of a new particle in the search for the Standard Model Higgs boson with the ATLAS detector at the LHC", *Phys.Lett.B* (2012) doi:10.1016/j.physletb.2012.08.020, arXiv:1207.7214.

[2] CMS Collaboration, "Observation of a new boson at a mass of 125 GeV with the CMS experiment at the LHC", *Phys.Lett.B* (2012) doi:10.1016/j.physletb.2012.08.021, arXiv:1207.7235.

[3] F. Englert and R. Brout, "Broken symmetry and the mass of gauge vector mesons", *Phys. Rev. Lett.* **13** (1964) 321, doi:10.1103/PhysRevLett.13.321.

[4] P. W. Higgs, "Broken symmetries, massless particles and gauge fields", *Phys. Lett.* **12** (1964) 132, doi:10.1016/0031-9163(64)91136-9.

[5] P. W. Higgs, "Broken symmetries and the masses of gauge bosons", *Phys. Rev. Lett.* **13** (1964) 508, doi:10.1103/PhysRevLett.13.508.

[6] G. S. Guralnik, C. R. Hagen, and T. W. B. Kibble, "Global conservation laws and massless particles", *Phys. Rev. Lett.* **13** (1964) 585, doi:10.1103/PhysRevLett.13.585.

[7] P. W. Higgs, "Spontaneous symmetry breakdown without massless bosons", *Phys. Rev.* **145** (1966) 1156, doi:10.1103/PhysRev.145.1156.

[8] T. W. B. Kibble, "Symmetry breaking in non-Abelian gauge theories", *Phys. Rev.* **155** (1967) 1554, doi:10.1103/PhysRev.155.1554.

[9] CDF and D0 Collaborations, "Evidence for a particle produced in association with weak bosons and decaying to a bottom-antibottom quark pair in Higgs boson searches at the Tevatron", *Phys.Rev.Lett.* **109** (2012) 071804, doi:10.1103/PhysRevLett.109.071804, arXiv:1207.6436.

[10] CDF Collaboration, "Combined search for the standard model Higgs boson decaying to a bb pair using the full CDF data set", *Phys.Rev.Lett.* **109** (2012) 111802, doi:10.1103/PhysRevLett.109.111802, arXiv:1207.1707.

[11] D0 Collaboration, "Combined search for the standard model Higgs boson decaying to $b\bar{b}$ using the D0 Run II data set", *Phys.Rev.Lett.* **109** (2012) 121802, doi:10.1103/PhysRevLett.109.121802, arXiv:1207.6631.

[12] CMS Collaboration, "Search for the standard model Higgs boson produced in association with W or Z bosons, and decaying to bottom quarks for ICHEP 2012", *CMS Physics Analysis Summary* **CMS-PAS-HIG-12-019** (2012).

[13] B. P. Roe, H.-J. Yang, and J. Zhu, "Boosted decision trees, a powerful event classifier",. Prepared for PHYSTATO5: Statistical Problems in Particle Physics, Astrophysics and Cosmology, Oxford, England, United Kingdom, 12-15 Sep 2005.

[14] GEANT4 Collaboration, "GEANT4: A Simulation toolkit", *Nucl. Instrum. Meth.* **A506** (2003) 250, doi:10.1016/S0168-9002(03)01368-8.

[15] S. Frixione, P. Nason, and C. Oleari, "Matching NLO QCD computations with Parton Shower simulations: the POWHEG method", *JHEP* **11** (2007) 070, doi:10.1088/1126-6708/2007/11/070, arXiv:0709.2092.

[16] S. Gieseke, D. Grellscheid, K. Hamilton et al., "Herwig++ 2.0 Release Note", (2006). arXiv:hep-ph/0609306.

[17] T. Sjöstrand et al., "PYTHIA", *Comput. Phys. Commun.* **135** (2001) 238.

[18] J. Alwall, M. Herquet, F. Maltoni et al., "MadGraph 5 : Going Beyond", *JHEP* **1106** (2011) 128, arXiv:1106.0522.

[19] J. Pumplin, D. R. Stump, J. Huston et al., "New generation of parton distributions with uncertainties from global QCD analysis", *JHEP* **0207** (2002) 012, arXiv:hep-ph/0201195.

[20] CMS Collaboration, "Measurement of the Underlying Event Activity at the LHC with $\sqrt{s} = 7$ TeV and Comparison with $\sqrt{s} = 0.9$ TeV", *JHEP* **1109** (2011) 109, doi:10.1007/JHEP09(2011)109, arXiv:1107.0330.

[21] CMS Collaboration, "Particle–Flow Event Reconstruction in CMS and Performance for Jets, Taus, and $E_{\mathrm{T}}^{\mathrm{miss}}$", CMS Physics Analysis Summary CMS-PAS-PFT-09-001, (2009).

[22] M. Cacciari, G. P. Salam, "Pileup subtraction using jet areas", *Phys. Lett. B* **659** (2008) 119, doi:10.1016/j.physletb.2007.09.077, arXiv:0707.1378.

[23] M. Cacciari and G. P. Salam and G. Soyez, "The anti-k_t jet clustering algorithm", *JHEP* **04** (2008) 063, doi:10.1088/1126-6708/2008/04/063, arXiv:0802.1189.

[24] M. Cacciari, G. P. Salam and G. Soyez, "FastJet user manual",. arXiv:hep-ph/1111.6097v1.

[25] M. Cacciari and G. P. Salam, "Dispelling the N^3 myth for the k_t jet-finder", *Phys. Lett. B* **641** (2006) 57, doi:10.1016/j.physletb.2006.08.037, arXiv:hep-ph/0512210.

[26] CMS Collaboration, "Determination of Jet Energy Calibration and Transverse Momentum Resolution in CMS", *JINST* **6** (2011) 11002, doi:10.1088/1748-0221/6/11/P11002.

[27] CMS Collaboration, "Electron Reconstruction and Identification at $\sqrt{s} = 7$ TeV", CMS Physics Analysis Summary CMS-PAS-EGM-10-004, (2010).

[28] CMS Collaboration, "Performance of CMS muon reconstruction in pp collision events at sqrt(s) = 7 TeV", *JINST* **7** (2012) P10002, doi:10.1088/1748-0221/7/10/P10002, arXiv:1206.4071.

[29] CMS Collaboration, "Algorithms for b jet identification in CMS", *CMS Physics Analysis Summary* **CMS-PAS-BTV-09-001** (2009).

[30] CMS Collaboration, "Measurement of btagging efficiency using ttbar events", *CMS Physics Analysis Summary* **CMS-PAS-BTV-11-003** (2011).

[31] J. M. Butterworth et al., "Jet Substructure as a New Higgs-Search Channel at the Large Hadron Collider", *Phys. Rev. Lett.* **100** (2008) 242001, doi:10.1103/PhysRevLett.100.242001.

[32] T. Aaltonen, A. Buzatu, B. Kilminster et al., "Improved b-jet Energy Correction for $H \to b\bar{b}$ Searches at CDF", (2011). arXiv:1107.3026.

[33] A. Hoecker et al., "TMVA - toolkit for multivariate data analysis", arXiv:0703039.

[34] CMS Collaboration, "Search for the standard model Higgs boson decaying to bottom quarks in pp collisions at", *Physics Letters B* **710** (2012), no. 2, 284, doi:10.1016/j.physletb.2012.02.085.

[35] J. Gallicchio and M. D. Schwartz, "Seeing in Color: Jet Superstructure", *Phys. Rev. Lett.* **105** (Jul, 2010) 022001, doi:10.1103/PhysRevLett.105.022001.

[36] CMS Collaboration, "Absolute Calibration of the CMS Luminosity Measurement: Summer 2011 Update", CMS Physics Analysis Summary CMS-PAS-EWK-11-001, (2011).

[37] CMS Collaboration, "Absolute Calibration of the Luminosity Measurement at CMS: Winter 2012 Update", CMS Physics Analysis Summary CMS-PAS-SMP-12-008, (2012).

[38] LHC Higgs Cross Section Working Group, S. Dittmaier, C. Mariotti et al., "Handbook of LHC Higgs Cross Sections: 1. Inclusive Observables", (CERN, Geneva, 2011). arXiv:1101.0593.

[39] M. Botje, J. Butterworth, A. Cooper-Sarkar et al., "The PDF4LHC Working Group Interim Recommendations", (2011). arXiv:1101.0538.

[40] S. Alekhin, S. Alioli, R. D. Ball et al., "The PDF4LHC Working Group Interim Report", (2011). arXiv:1101.0536.

[41] H.-L. Lai, M. Guzzi, J. Huston et al., "New parton distributions for collider physics", *Phys. Rev. D* **82** (2010) 074024, doi:10.1103/PhysRevD.82.074024, arXiv:1007.2241.

[42] A. D. Martin, W. J. Stirling, R. S. Thorne et al., "Parton distributions for the LHC", *Eur. Phys. J. C* **63** (2009) 189, doi:10.1140/epjc/s10052-009-1072-5, arXiv:0901.0002.

[43] NNPDF Collaboration, "Impact of Heavy Quark Masses on Parton Distributions and LHC Phenomenology", *Nucl. Phys. B* **849** (2011) 296, doi:10.1016/j.nuclphysb.2011.03.021, arXiv:1101.1300.

[44] M. Ciccolini et al., "Strong and electroweak corrections to the production of Higgs+2jets via weak interactions at the LHC", *Phys. Rev. Lett.* **99** (2007) 161803, doi:10.1103/PhysRevLett.99.161803, arXiv:0707.0381.

[45] M. Ciccolini, A. Denner, and S. Dittmaier, "Electroweak and QCD corrections to Higgs production via vector-boson fusion at the LHC", *Phys. Rev.* **D77** (2008) 013002, doi:10.1103/PhysRevD.77.013002, arXiv:0710.4749.

[46] A. Denner, S. Dittmaier, S. Kallweit et al., "Electroweak corrections to Higgs-strahlung off W/Z bosons at the Tevatron and the LHC with HAWK", 2011.

[47] G. Ferrera, M. Grazzini, and F. Tramontano, "Associated WH production at hadron colliders: a fully exclusive QCD calculation at NNLO", arXiv:1107.1164.

[48] CMS Collaboration, "Measurement of the single-top t-channel cross section in pp collisions at centre-of-mass energy of 8 TeV", *CMS Physics Analysis Summary* **CMS-PAS-TOP-12-011** (2012).

[49] A. L. Read, "Presentation of search results: the CLs technique", *J. Phys. G* **28** (2002) 2693, doi:10.1088/0954-3899/28/10/313.

[50] T. Junk, "Confidence level computation for combining searches with small statistics", *Nucl. Instrum. Meth.* **A434** (1999) 435, doi:10.1016/S0168-9002(99)00498-2.

[51] ATLAS and CMS Collaborations, LHC Higgs Combination Group, "Procedure for the LHC Higgs boson search combination in Summer 2011", ATL-PHYS-PUB/CMS NOTE 2011-11, 2011/005, (2011).

[52] CMS Collaboration, "Search for Higgs Boson in VH Production with H to bb", *CMS Physics Analysis Summary* **CMS-PAS-HIG-11-031** (2011).